HHS Public Access

Author manuscript

Nat Cell Biol. Author manuscript; available in PMC 2011 June 01.

Published in final edited form as:

Nat Cell Biol. 2010 December ; 12(12): 1133–1142. doi:10.1038/ncb2124.

Tissue elongation requires oscillating contractions of a basal actomyosin network

Li He[1,*], **Xiaobo Wang**[1,*], **Ho Lam Tang**[1], and **Denise J. Montell**[1,3]

[1] Department of Biological Chemistry, Center for Cell Dynamics, Johns Hopkins School of Medicine, 855 North Wolfe Street, Baltimore, MD 21205 USA

Abstract

Understanding how molecular dynamics lead to cellular behaviors that ultimately sculpt organs and tissues is a major challenge not only in basic developmental biology but also in tissue engineering and regenerative medicine. Here we use live imaging to show that the basal surfaces of *Drosophila* follicle cells undergo a series of directional, oscillating contractions driven by periodic myosin accumulation on a polarized actin network. Inhibition of the actomyosin contractions or their coupling to extracellular matrix (ECM) blocked elongation of the whole tissue, whereas enhancement of the contractions exaggerated it. Myosin accumulated in a periodic manner prior to each contraction and was regulated by the small GTPase Rho, its downstream kinase ROCK and cytosolic calcium. Disrupting the link between the actin cytoskeleton and the ECM decreased, while enhancing cell-ECM adhesion increased, the amplitude and period of the contractions. In contrast, disrupting cell-cell adhesions resulted in loss of the actin network. Our findings reveal a novel mechanism controlling organ shape and a new model for the study of the effects of oscillatory actomyosin activity within a coherent cell sheet.

Introduction

The goal of tissue engineering is to create artificial organs and tissues *in vitro*, which requires understanding not only how each cell type is specified but also how cells cooperate to generate appropriate organ shapes and tissue architectures. The molecular and mechanical mechanisms governing some multicellular morphogenetic movements are beginning to be elucidated[1], [2]. For example, periodic contraction of apical networks of actomyosin in *Drosophila* embryos drives apical constriction, which contributes to many morphogenetic movements including mesoderm invagination and dorsal closure. In addition, apical accumulation of myosin specifically at dorsal-ventral (D-V) cell-cell boundaries drives directional cell intercalation during germ band elongation[3]–[5]. A remaining challenge is to

[3]To whom correspondence should be addressed: dmontell@jhmi.edu.

[*]These authors contributed equally

Author Contributions

The image acquisition and mutant analysis were carried out by L. H. and X. W. Images were processed and analyzed by L. H. Inhibitor treatments and calcium related experiments were carried out by H. L. T. The manuscript was prepared by D. J. M. All authors participated in interpretation of the data and production of the final manuscript.

explain the great diversity of morphogenetic processes that occur, and in particular those that do not involve apical constriction. Oogenesis in Drosophila serves as a good model system to study a variety of cell behaviors during morphogenesis[6, 7].

The *Drosophila* ovary is made up of developing egg chambers, each of which produces a single egg. Each egg chamber is composed of 16 germline cells (15 nurse cells and 1 oocyte) surrounded by a monolayer of epithelial follicle cells (Supplementary Information, Fig.S1a). From developmental stage 8 to late stage 10, the egg chamber grows dramatically, increases in volume ~8-fold, and elongates ~1.7-fold. The cellular and molecular mechanisms regulating the elongation of this tissue are incompletely understood, and contradictory models have been proposed. Apical constriction has been suggested to play a role[8]; however, a quantitative analysis of follicle cell structure found no evidence that apical constriction occurs[9]. The latter study suggested that the increase in egg chamber volume combined with a "corset" to constrain the volume increase to the ends of the tissue could account for egg chamber elongation. Follicle cells acquire a polarized array of F-actin near the basal surface, which aligns with extracellular matrix fibers, possibly contributing to the corset since disruption of cell-matrix adhesion can cause eggs to be rounder[10–13]. However, all previous studies of this process have relied upon analysis of fixed tissue, and thus no dynamic information has been available to assist in elucidating the mechanism.

Results

Basal cell surface area oscillation correlated with myosin accumulation in Drosophila follicle cells

To understand this tissue elongation process better, we used egg chamber culturing techniques and live imaging[14, 15] of E-cadherin fused to GFP (Cadherin-GFP)[16] to observe dynamic changes in the egg chamber between stages 8 and 10 (Fig. 1a–k; Supplementary Information, Fig.S1b j, and Movie 1). During time-lapse imaging, basal cell surfaces exhibited periodic contraction and relaxation (Fig. 1l, m; Supplementary Information Movie 2). In contrast, apical surfaces showed smaller, random changes (Supplementary Information Movie 3).

The basal oscillations bore some resemblance to recently observed pulsation during apical constriction in *Drosophila* embryos[3, 4, 17–20], which is caused by a periodic accumulation and contraction of apical actomyosin. Therefore we monitored myosin accumulation using the red fluorescent protein mcherry fused to the myosin regulatory light chain named Spaghetti Squash (Sqh-mcherry)[3]. From still images, apical myosin resembled a random mesh (Fig. 1g, h), whereas basal myosin accumulated in parallel fibers near the basal follicle cell surface with highly variable intensity (Fig. 1j, k). Time-lapse imaging revealed that the variation in intensity was due to repeated cycles of basal myosin accumulation and disappearance from individual cells (Fig. 1n), which were asynchronous. There seemed to be a correlation between myosin accumulation and basal cell surface area reduction within each cell (Fig. 1l–n, Supplementary Information, Movie 2).

Quantification and comparison of basal and apical follicle cell activities

To quantify these effects, we developed a MATLAB program to automatically track the change of cell geometry and found that the basal area indeed showed clear periodic changes (Fig. 2a). The basal area change was highly polarized, correlating with a change in the length of cells along the D-V axis whereas we observed little or no change in cell length along the anterior-posterior (A-P) axis (Fig. 2a). The average period of the basal contractions was 6.3 minutes with most contraction-relaxation cycles completed in 5~7 minutes (Fig. 2b). In contrast apical cell surfaces showed small, random fluctuations in cell shape (Fig. 2c and Supplementary Information, Movie 3), which were only half the magnitude of the change of the basal surface area (Fig. 2d). The apical area change was also symmetric while the basal membrane activity was 5-fold higher in the D-V than in A-P the direction (Fig. 2e).

In time lapse movies, basal myosin underwent dramatic and periodic changes in concentration (Fig. 2g, h and Supplementary Information, Movie 2), whereas near the apical surface, myosin showed no periodicity (Fig. 2c, h) and was far less dynamic (Fig. 2f). A lateral view showed that myosin accumulated in and then disappeared from a thin layer ~1 μm beneath the basal plasma membrane, rather than moving into and out of the basal plane of focus (Supplementary Information, Movie 4).

Simultaneous measurement of basal myosin accumulation and cell area showed that the area shrank as myosin accumulated (Fig. 2g; Supplementary Information, Fig.S1k), supporting the two phenomena might be related. The rate of myosin accumulation correlated well with the rate of contraction of the cell area (Fig. 2g), the former preceding the latter by about one minute, suggesting that myosin accumulation could in principle cause the reduction in basal surface area.

Basal actin organization

We then used GFP tagged-Moesin, an F-actin binding protein, to visualize dynamic changes of F-actin[21]. As previously reported[10], F-actin forms parallel bundles along basal follicle cell surfaces (Fig. 3a, b). However, in contrast to the periodic ~70% changes in myosin concentration, actin filament density changed by only ~20% over time (Fig. 3c, Supplementary Information, Movie 5). A time correlation analysis showed that, in contrast to the myosin accumulation, the change in F-actin did not precede but rather coincided with the change in myosin intensity (Fig. 3d–g). Together these results suggest that the periodic changes in myosin accumulation were not caused by dynamic changes in F-actin.

While the periodic myosin accumulation and cell surface area reductions described here resemble the pulsatile contractions that underlie apical constriction during *Drosophila* gastrulation[3, 4, 18–20], the activity in follicle cells differs in several key respects (Fig. 3j). Firstly, the follicle cell contractions occur near the basal cell surface rather than apically. Secondly, during apical constriction myosin fibers accumulate in a randomly oriented meshwork[3], whereas basal myosin fibers in follicle cells were highly organized in parallel bundles along the D-V axis (Supplementary Information, Movie 5 and Fig. 3j). Thirdly, the actin filaments change intensity with similar amplitude as myosin in apical constriction[20],

while there is little change in basal actin in follicle cells (Supplementary Information, Movie 5 and Fig. 3j). Fourthly, the reduction in apical surface area in the embryo is eventually stabilized by a poorly characterized ratchet mechanism, resulting in a lasting change in cell shape, whereas the change in basal follicle cell shape was temporary (Fig. 3h, i and Supplementary Information, Fig.S2a-j). Finally in the gastrulating embryo the contractions are limited to cells on the ventral side of the embryo whereas the follicle cell activity was symmetrical with respect to the D-V axis of the egg chamber.

Spatial and temporal regulation of periodic myosin accumulation

Although the basal oscillations were not patterned along the D-V axis, we did notice a global spatial and temporal pattern to the myosin accumulation and cellular contractions (Fig. 4a–e, Supplementary Information, Movie 6). The myosin oscillations appeared first in early stage 9 in a band of cells about 1/3 of the distance from the anterior pole and shifted relatively quickly to the middle part of the egg chamber (Fig. 4a, b). During development, both the average basal myosin intensity and the number of oscillating cells increased until stage 10, by which time almost all follicle cells in contact with the oocyte accumulated basal myosin (Fig. 4b–f), whereas apical myosin changed very little over the same developmental stages (Fig. 4g–k). Nurse cell associated follicle cells never displayed measurable myosin accumulation (Fig. 4b–e).

Actomyosin contraction regulates tissue shape

Since the myosin oscillations and overall tissue elongation occur during the same stages of development (Fig. 4a), we hypothesized that the periodic contractions might contribute to tissue elongation. To test this hypothesis, we first took a pharmacological approach to interfere with actin and myosin function (Supplementary Information, Movie 7). Compared with control samples treated with DMSO (Fig. 5a, d, h), addition of cytochalasin D (cytoD), an actin filament destabilizer, greatly reduced the basal actin and myosin filaments and blocked the oscillations (Fig. 5b, e, h). Interestingly, this also resulted in a clear relaxation and expansion of egg chamber width (Fig. 5b, g). In contrast, addition of the calcium ionophpore ionomycin, which promotes contraction of actomyosin filaments in smooth muscle cells[22], [23], dramatically increased the amount of basal myosin (Fig. 5f, h) and elongated the egg chamber (Fig. 5c, g and Supplementary Information, Movie 7). In contrast, the microtubule destabilizer colchicine had no effect on the myosin oscillation, but did deform the tissue, resulting in irregularly shaped egg chambers (Supplementary Information, Fig.S3j). Apical actin and myosin showed similar changes in response to CytoD and ionomycin treatment (Supplementary Information, Fig 3d–g), so this experiment did not rule out a contribution of the apical cytoskeleton; however the lack of polarization and dynamics made the apical cytoskeleton a poorer candidate for involvement in this directional tissue elongation. Taken together these findings indicate that a contracting actomyosin network generates active forces to restrict the width of the tissue resulting in its elongation (Fig. 5g, i).

Effect of Rho-ROCK pathway and cell-adhesion on myosin assembly and tissue shape

To explore the molecular mechanisms regulating actomyosin contractility further, we tested the function of the small GTPase Rho, which regulates actin stress fiber formation and

myosin contractility in other contexts[24], and its effector Rho kinase (ROCK) (Supplementary Information, Movie 8). Clones of follicle cells expressing a dominant negative form of Rho (RhoN19) failed to accumulate basal myosin whereas neighboring wild type follicle cells did so normally (Fig. 6a, b, i). In contrast, cells expressing the constitutively active form RhoV14 maintained a constant high level of basal myosin (Fig. 6c, i) and failed to relax (Supplementary Information, Movie 8). We then investigated the Rho effector kinase ROCK, which can activate myosin[24]. Cells expressing a ROCK RNAi construct, like RhoN19-expressing cells, lost basal myosin (Fig. 6d, i) and stopped oscillating (Supplementary Information, Movie 8), as did cells in egg chambers treated with the ROCK inhibitor Y-27632[25] (Supplementary Information, Fig.S3a, k, p). Global knockdown of ROCK in all follicle cells also made the egg chamber rounder than the control (Fig. 6j–m, r), without any overall change of epithelium architecture. More importantly, apical actomyosin was little affected by ROCK RNAi, supporting the notion that the basal contraction was responsible for the effect (Fig. 6i, Supplementary Information, Fig. S4h, S5h, q).

The parallel basal actin filaments are essential for egg chamber elongation[13], [26–29]. Alignment of these filaments and ECM fibers has been suggested to function as a "molecular corset", restricting the increase in tissue volume to the ends of the egg chamber[10–12], [27]. Blocking integrin-mediated adhesion of follicle cells to the ECM also disrupts egg chamber elongation[13], [26]. Therefore, we investigated the relationship between basal contractions and the cell-ECM interaction. To test the effect of cell-matrix adhesion on basal follicle cell oscillations, we knocked down expression of talin, which is essential for integrin-mediated adhesion[30]. Basal myosin intensity decreased by 50% percent in mutant follicle cells (Fig. 6e, i and Supplementary Information, Movie 9). Paxillin is also an important linker between integrin and F-actin, over-expression of which enhances cell-matrix adhesion[31], [32], and we found that paxillin over-expression increased myosin intensity by 60% (Fig. 6f, i and Supplementary Information, Movie 9). Neither talin knock-down nor paxillin over-expression had any detectable effect on the apical actomyosin network (Fig. 6i, Supplementary Information, Fig. S4j, l, S5j, l, q). Global talin knockdown caused a round egg phenotype (Fig. 6n, o, r) while paxillin over-expression elongated egg chambers (Fig. 6p, q, r), consistent with their respective changes in basal myosin intensity.

We then tested whether cell-cell adhesion had any effect on the basal oscillation. Although cadherin is markedly enriched in sub-apical adherens junctions between follicle cells, it is also present all over basolateral cell surfaces including at the level of the basal actin filament bundles (Supplementary Information, Fig. S6k). Cells expressing E-cadherin RNAi lost the basal actin and myosin filaments (Fig. 6g, i and Supplementary Information, Fig. S4m, n, S5m, n, q), whereas over-expression of E-cadherin caused no detectable effect (Fig. 5h, i). Thus the basal actin network requires cadherin mediated cell-cell adhesion, similar to basal actin stress fibers in cultured endothelial cells[33].

Cell autonomy and regulation of amplitude and period of the basal oscillations

In the mosaic analysis, we noticed that wild type cells surrounded by either constitutively relaxing (expressing RhoN19 or ROCK RNAi) or contracting (expressing RhoV14)

neighboring cells still oscillated with normal amplitude and period, demonstrating that the basal oscillation is a cell-autonomous behavior (Fig 7. a–d and Supplementary Information, Movie 8).

To investigate the factors controlling the amplitude or period of the basal oscillations, we changed the extracellular or cytosolic calcium concentration or applied different concentrations of the ROCK inhibitor Y-27632. Buffering of extracellular calcium with EGTA did not alter the myosin oscillations (Supplementary information Fig. S3h, i, p). However buffering intracellular calcium with BAPTA decreased the myosin intensityand increasing intracellular calcium with ionomycin had the opposite effect (Supplementary information Fig. S3i and S3n–p). Although the basal myosin intensity changed dramatically, as long as there was still a detectable oscillation, the period remained largely unchanged (Fig. 7e, f). This was consistent with the observation that in wild type tissue, follicle cells at different positions or developmental stages exhibit different amplitudes of myosin oscillation, but similar periods (Fig. 7g). This result implies that while ROCK activity and presence of proper cytosolic calcium are necessary for maximal myosin accumulation, they may not be essential components of the oscillator. In contrast, altering integrin-mediated cell-ECM adhesion, changed the oscillation period together with myosin amplitude. Cells expressing talin RNAi exhibited a shorter period (4 min on average) while cells over-expressing Paxillin exhibit a longer period (9.3 min on average) (Fig. 7h–j). These results suggest that increasing cell-matrix adhesion slows the period of the oscillator, possibly by providing more mechanical resistance.

Discussion

We describe a novel behavior of epithelial cells, specifically a patterned, oscillating, basal epithelial myosin assembly and contraction. Previous work suggested that the polarized, basal F-actin bundles and their integrin-mediated attachment to the surrounding basement membrane function as a corset, implying a static structure, that constrains growth of the egg chamber to the poles thus promoting tissue elongation[10–12]. Here we show that, surprisingly, the “corset” is dynamic and is composed of periodic assembly and disassembly of myosin on the actin filaments, providing an explanation for the source of the necessary force. Contraction transiently diminishes the basal surface area of the affected follicle cells, however this is not permanent, and we propose that it is not the most significant consequence of the contraction. Instead, the force generated by the contraction propagates inward toward the germline and opposes the outward force caused by growth. Since the oscillations occur near the center of the egg chamber, expansion is directed preferentially to the poles. The oscillations are not synchronized, therefore different cells contract at different times and over the course of more than ten hours generate a sustained inward force.

These observations raise a number of interesting questions. For example, what is the biochemical mechanism of the oscillation? Myosin activity oscillates in many (but not all) biological contexts. For example cardiomyocytes beat in cell culture. However this oscillation does not display or require cycles of myosin assembly and disassembly, is driven by ion fluxes, and is much more rapid (150 beats per min) than the oscillations described here (average period of 6–7 minutes). Intriguingly, myosin has intrinsic biochemical

properties that could in principle lead to oscillating assembly and disassembly on this time scale[34]. Three properties, in combination, could contribute to oscillation: the intrinsic mechanochemical cycle of actin binding, power stroke, and dissociation from actin; thick filament assembly-disassembly dynamics; and actin filament anchoring. Myosin II assembly into thick filaments is tension-dependent[35,36]. That is, as myosin begins to assemble on actin filaments, it exerts force upon them, generating tension if the filaments are anchored. If the resistance is great enough, myosin will stall in the isometric state rather than completing its power stroke and disassociating from the actin filament [34]. As a consequence, more and more myosin filaments assemble over time. In addition, myosin binding to actin becomes highly cooperative in response to tension. Thus more myosin molecules bind and they dissociate more slowly when there is tension. For myosin to sense and respond to tension, the actin filaments to which it is bound must be prevented from sliding. During Dictyostelium cytokinesis, the critical actin anchor is the actin crosslinker cortexillin[37]. However in principle anchoring to the plasma membrane could also serve this purpose. In Drosophila follicle cells we found that myosin assembles on F-actin stress fibers that are attached via integrin, talin and paxillin to ECM fibers. This likely serves the critical function of anchoring actin filaments so that tension is generated when myosin binds. So what causes disassembly and leads to oscillations? When enough myosin molecules assemble such that the force per myosin head becomes small enough, then the myosins can complete their power strokes and disassociate from actin, resulting in myosin thick filament disassembly. Stochastically, new myosins bind, exert force, experience tension, recruit more myosin and the cycle repeats.

Increasing the load against which myosin works would be expected to increase the number of myosin molecules that assemble as well as the length of time until the force per unit molecule reduces to the point of disassembly. In other words increasing the mechanical resistance should increase both the amplitude and period of myosin oscillations. Our results suggest that the actin-integrin-ECM interaction provides the load, and explains why decreasing follicle cell-ECM adhesion reduces both the period and amplitude of the oscillation and why enhancing cell-ECM interaction increases both. This explanation is also consistent with the observation that the assembly-disassembly cycle that occurs during ventral furrow formation in the embryo has a shorter period (~1 minute). In this case the cycle occurs on the apical side of the cell where there is no basement membrane to provide mechanical resistance. Although there may be additional components to the oscillation mechanism, these elements would be sufficient in principle to cause oscillating myosin assembly and disassembly.

In contrast to most previously studied morphogenetic processes, in which cells change the shape of a tissue by altering their own geometry, follicle cells undergoing this basal contraction do not change their own shape permanently, but rather generate forces that constrain the shape of the underlying tissue (Fig. 8). Another morphogenetic process that involves two cell layers is branching morphogenesis of the developing mammary gland[38]. In this case outer myoepithelial cells may help sculpt the underlying glandular epithelium constraining growth toward the terminal end buds. It will be of interest to determine whether basal actomyosin activity in the epithelial layer also contributes to the morphogenesis of this or other organs and tissues where expansion is constrained.

The observation that this oscillation shares some characteristics with other actomyosin oscillations, such as that occurring during apical constriction, and yet differs in numerous respects, suggests that an intrinsic oscillator is subject to tissue specific regulation. This allows the oscillations to occur in some cells and at some stages of development but not others, near the apical cell surface in some cells or the basal side in others, and connected to a ratchet in some cells but not others. In addition, the period can be regulated in a cell-type specific manner by adjusting the resistance against which the motor pulls. In each cell type where it has been described, the observation of oscillations came as a surprise since intuitively a static contractile force might seem to suffice. Whether or not oscillation is essential remains to be clarified. In any case, a complete understanding of the temporal and spatial patterning, subcellular localization, and tuning of the oscillations will be necessary in order to realize the goal of reconstituting normal organ shapes and tissue architectures *in vitro*.

Methods

Drosophila stocks and genetics

The following fly stocks were used: Ubi::DE-cadherin-GFP and sqh::sqh-mcherry (from Dr. Eric F. Wieschaus), UAS-Moesin-GFP, UAS-RhoN19, UAS-RhoV14 (from Bloomington Drosophila Stock Center), UAS-DE-cadherin^{RNAi}, UAS-ROCK^{RNAi} and UAS-talin^{RNAi} (from Vienna Drosophila RNAi Center[39]), UAS- GFP-paxillin. *hs*Gal4/CyO, MKRS/TM6B flies were used to express UAS lines in all follicle cells. Clones were generated using FLP-OUT technique by crossing UAS transgenic flies with either P[*hsp*70-flp]; sqh::sqh-mcherry; UAS-mcd8GFP, *Ay*Gal4 or P[hsp70-flp]; UAS-nlsGFP, *Ay*Gal4; sqh::sqh-mcherry. For fixed sample, FLP-OUT fly without sqh::sqh-mcherry was used. All stocks and crosses were maintained at room temperature. *hs*FLPase was induced at 37°C for 1hr and flies were then kept at either 29°C or 31°C for 2 days before dissection. hsGal4 were induced three times at 37°C for 1hr each and flies were kept at 25°C for 1~2 days before dissection.

DNA constructs and transgenic fly generation

Full length paxillin cDNA was obtained from *Drosophila* Genomics Resource Center and amplified by following primers: GGGGACAAGT TTG TACAAAAAAGCAGGC TTCAACATG GACGATTTG GATGCTCTAT (5 end) and GGGGACCACTTTGTACAAGAAAGCTGGGTGTCATCCGAATATCTTGTCGAAG CAG (3 end). The PCR product was first cloned into pDONR™221 vector (Invitrogen) using BP clonase™II (Invitrogen). Then the insertion was recombined into pUASt gateway vector with N-fusion of GFP (from DGRC) by LR clonase™II (Invitrogen). UAS-GFP-paxillin flies were generated by Bestgene Inc. using w^{1118} fly. Flies with UAS-GFP-paxillin was crossed with *hs*Gal4; sqh::sqh-mcherry flies to test expression pattern and level. Expressed GFP-paxillin enriched at the focal adhesion site as previously reported[40] (Supplementary Information, Fig. S6j).

Time-lapse image acquisition

Drosophila egg chambers were dissected and mounted in live imaging medium (Invitrogen Schneider's insect medium with 20% FBS and 0.1 mg/ml insulin) as previously described[14], [15]. Egg chambers were slightly compressed to overcome the endogenous curvature. More glass spacers were used when capturing z-stack images of egg chambers without compression (Fig. 1a, b, Supplementary Information, Movie 1). The basal oscillation pattern, intensity and period were similar in both conditions. Fixed samples showed a similar pattern suggesting that the myosin pattern is not an artifact of the culture condition (Supplementary Information, Fig. S1c-j). Time-lapse-imaging was carried out on Zeiss 710 NLO-Meta confocal microscope using 40X, N.A.1.1 water immersion lens, with 488nm argon laser and a 543nm green HeNe laser. Imaging with 10 sec intervals was tested at first. Because the average oscillation period is 6.3 min, we used 60 sec interval to prolong the imaging time for most of experiments unless specified otherwise.

Basal focal plane, which is ~1μm beneath the basal surface, was selected during live imaging to maximize the basal myosin intensity. When imaging the apical side, the focal plane was selected based on the clearest cadherin-GFP signal. The same microscope setup was used when comparing intensity among different samples.

Image processing and data analysis

For all images background (intensity of area without sample) was subtracted. All displaced figures were processed by a Gaussian smoothing filter with a radius of one pixel to reduce noise. 3D reconstructions of egg chambers were generated by maximum projection (Supplementary Information, Movie 1) or transparent projection (to highlight the surface, Fig. 1a, c) from Z-stacks with 1μm interval using Zeiss ZEN (http://www.zeiss.de/zen).

Time-lapse Cadherin-GFP images were processed using Image J as follows: images were first filtered by a Gaussian blur filter with radius of 25 pixels, the resulting images were subtracted from original images as local background, then the images were segmented by watershed algorithm plug-in[41]. The segmented images were corrected manually based on the original images.

The processed images were analyzed by MATLAB (MathWorks) to track individual cells and automatically calculate the cell area, Anterior-Posterior (A-P) length and Dorsal-Ventral (D-V) length. A-P and D-V length were calculated by averaging the edge distance in each direction. Sqh-mcherry channel was processed in MATLAB first to correct for photobleaching. Subsequently intensity of an individual cell was calculated as the average value of all pixels within the cell area. A general cytosolic myosin signal contributed to the final results and represents ~20% of the average myosin signal.

For myosin (red), moesin (green) dual-color imaging, the intensity of Moesin-GFP or Sqh-mcherry was calculated from manually outlined cell areas as was the myosin intensity in mutant clones since cadherin-GFP was not present to mark cell boundaries.

The distribution of oscillation periods was generated by measuring the intervals between each pair of adjacent peaks. The myosin signals were used because they were less noisy than

surface area. We applied autocorrelation to calculate the period of a time series with different time offsets. The location of the first peak greater than zero indicates the shortest period contained in the series. This method averages out irregularities in the sequence and gives similar average period (Fig. 2h). We found autocorrelation is more robust and provides better result in analyzing irregular signals with small amplitude, such as the myosin intensity in talinknock-down cells (Fig. 7h-j). Therefore, analysis of period in all experiment other than Fig. 1p was calculated by the autocorrelation.

The time series data was smoothed by a Gaussian filter with σ equal to 3 data points. The basal contraction rate was calculated as the inverse value of the first derivative of basal area. The rate of intensity change was the first derivative of intensity. Data for correlation was collected with 30 sec interval to catch subtle phase difference. Cross-correlation efficiency was calculated with time shift from -9 to +9 min. Heat-map was constructed by correlations from different individual cells with correlation coefficient coded in rainbow color. Averaged correlation coefficient was generated by averaging smoothened correlation data from tested cells.

Myosin intensity was analyzed using egg chambers from early to middle stage10 because of the widespread and reliable basal myosin pattern. Anterior columnar follicle cells were used in quantification because of their consistent behavior. The change of the one measured variable was defined as 2 s.d. above and 2 s.d. below the mean. Unpaired two-sided t-Test was carried out using EXCEL (Microsoft).

Small molecule and other treatments

Egg chambers were dissected in live imaging medium with chemicals at the indicated final concentration, and then mounted for imaging. The following chemicals and final concentrations were used: F-actin destabilizer Cytochalasin D (20μg/ml, sigma), Calcium ionophore Ionomycin (2.5μM, Invitrogen), microtubule destabilizer Colchicine (50μg/ml, sigma), ROCK inhibitor Y-27632 (200μM, sigma), cytosolic calcium chelator BAPTA-acetoxymethyl ester (50μM, Invitrogen). For BAPTA treatment, non-ionic detergent Pluronic® F-127 (Invitrogen) was applied to the medium at final concentration 0.02 % to facilitate dispersion of the AM ester in aqueous media. Sample was incubated with the BAPTA-AM and Pluronic® F-127 for 1 hour and then washed and recovered in BAPRA-AM free medium for another 15 min prior to microscopy. Quantification of egg chamber shape change after drug treatment used the images taken at the start (0 min) and the end (20 min) of live imaging (~10 min used in mounting and microscope preparation after adding drug not included). An image of the middle (sagittal) plane of the egg chamber was used. Tissue width was calculated by dividing the area of the posterior half of the egg chamber (the oocyte and its associated columnar follicle cells) by its A-P length

5% DMSO or ethanol (for Colchicine) was used as control. Effect of ionomycin can be blocked by adding 5mM EGTA or 200μM Y-27632 after 1 min incubation with ionomycin, while addition of 10mM EGTA had no immediate effect. Prolonged incubation with EGTA caused endocytosis of cadherin and loss of basal myosin. 2.5μM ionomycin immediately reversed the effect of BAPTA. The effect of treatment with Y-27632 can also be reversed by 2.5μM ionomycin together with 5mM $CaCl_2$.

Dosage dependent effects of ROCK inhibition on basal myosin was tested by applying different concentrations of Y-27632 (0–200μM) for 1hr before live imaging. To control Ca^{2+} concentration, component defined *Drosophila* Ringer's buffer (with 2mM Ca^{2+}) was used. Due to nutrient limitations egg chambers can survive for only ~2 hr in this medium, compared to ~6–8 hr in live imaging medium. However, the basal contraction appeared normal. Samples were first treated with 2.5μM ionomycin for 1 min followed by addition of different concentrations of EGTA, then immediately imaged for 30–50 minutes.

Immunohistochemistry

Drosophila ovaries were dissected in Schneider's medium and fixed with 4% formaldehyde for 20 minutes. Antibody staining was carried out as previously decribed[42]. Anti-talin antibody (1:100) was a gift from Dr. Brown, N. H.[30], anti-DE-cadherin antibody (rat anti-dCAD2, 1:10) and anti-Armadillo antibody (mouse N27A1, 1:50) were from Developmental Studies Hybridoma Bank. Secondary antibodies conjugated with Alex-568 and Alexa-647 were used in 1:300 dilutions (Molecular Probes). Alexa 568-conjugated phalloidin (1: 300, Invitrogen) was used for F-actin staining. Samples were imaged on Zeiss LSM 510-Meta confocal microscope.

RT-PCR analysis

*hs*Gal4;UAS-RNAi was used to knockdown the specific targets in all ovary follicle cells (Supplementary information Fig. S6a–i). Flies were treated with heat-shock at 37°C for 1 hour, 6 times over 2 days. After recovery for 1 day, total RNA was extracted from whole flies by RNeasy Mini kit (Qiagen 74104), and was quantified by measuring the A_{260}. For reverse transcription-PCR, 1 μg of RNA was reverse transcribed with Superscript RNase H-RT (Invitrogen) in the presence of 100 ng of oligo dT (Invitrogen). PCR for different targets was performed in a thermal cycler in the following cycle: 95°C 30 second, 55°C 30 second and 72°C 60 second; for 20–24 cycles in different primers reaction of E-cadherin, Rock or Talin. The actin primer reaction required 16 cycle. The following primers were used:

cadherin forward1: GGATACGCTCCTAAGGTCAA;

cadherin reverse1: CCGACTCCTTGTCAATCTTG;

cadherin forward2: GACGAGTGTCTGATTGAGAAG;

cadherin reverse2: ATCTTGGTGTTGTTGCAGGC;

Rock forward1: GAGAAACTGTGACCAAGCAG;

Rock reverse1: GAGAACCACCTCCATTGTGT;

Rock forward2: CAAGGACGAAGAGATCACCA;

Rock reverse2: CAATCGATCTCCATGACCAT;

Talin forward1: CATACAGTTCCAGCCCAACA;

Talin reverse1: TCTGCCTCATCTATTCCCTG;

Talin forward2: CAAACACCTTCACTCTGGAC;

Talin reverse2: TGCGAACTTCCTTAGTCGTG;

actin forward: GGAGAAGCTGTGCTATGTTG;

actin reverse: TGATGGAGTTGTAGGTGGTC;

Supplementary Material

Refer to Web version on PubMed Central for supplementary material.

Acknowledgments

We thank Dr. Doug Robinson for invaluable discussions, critical reading of the manuscript and help writing the discussion of the myosin oscillation mechanism. Drs. Nick Brown and Eric Wieschaus generously donated reagents. This work was supported by grants to D. J. M from NIGMS including R01 GM46425, GM and the Cell Migration Consortium. Bloomington Drosophila Stock Center and Vienna Drosophila RNAi Center resources contributed to this work. FlyBase provided important information used in this work. Clones provided by the BDGP and distributed by DGRC were used.

References

1. Lecuit T, Lenne PF. Cell surface mechanics and the control of cell shape, tissue patterns and morphogenesis. Nat Rev Mol Cell Biol. 2007; 8:633–44. [PubMed: 17643125]
2. Mammoto T, Ingber DE. Mechanical control of tissue and organ development. Development. 2010; 137:1407–20. [PubMed: 20388652]
3. Martin AC, Kaschube M, Wieschaus EF. Pulsed contractions of an actin-myosin network drive apical constriction. Nature. 2009; 457:495–9. [PubMed: 19029882]
4. Solon J, Kaya-Copur A, Colombelli J, Brunner D. Pulsed forces timed by a ratchet-like mechanism drive directed tissue movement during dorsal closure. Cell. 2009; 137:1331–42. [PubMed: 19563762]
5. Bertet C, Sulak L, Lecuit T. Myosin-dependent junction remodelling controls planar cell intercalation and axis elongation. Nature. 2004; 429:667–71. [PubMed: 15190355]
6. Horne-Badovinac S, Bilder D. Mass transit: epithelial morphogenesis in the Drosophila egg chamber. Dev Dyn. 2005; 232:559–74. [PubMed: 15704134]
7. Wu X, Tanwar PS, Raftery LA. Drosophila follicle cells: morphogenesis in an eggshell. Semin Cell Dev Biol. 2008; 19:271–82. [PubMed: 18304845]
8. Wang Y, Riechmann V. The role of the actomyosin cytoskeleton in coordination of tissue growth during Drosophila oogenesis. Curr Biol. 2007; 17:1349–55. [PubMed: 17656094]
9. Kolahi KS, et al. Quantitative analysis of epithelial morphogenesis in Drosophila oogenesis: New insights based on morphometric analysis and mechanical modeling. Dev Biol. 2009; 331:129–39. [PubMed: 19409378]
10. Gutzeit HO. The microfilament pattern in the somatic follicle cells of mid-vitellogenic ovarian follicles of Drosophila. Eur J Cell Biol. 1990; 53:349–56. [PubMed: 2081548]
11. Gutzeit HO, Eberhardt W, Gratwohl E. Laminin and basement membrane-associated microfilaments in wild type and mutant Drosophila ovarian follicles. J Cell Sci. 1991; 100 (Pt 4): 781–8. [PubMed: 1814932]
12. Gutzeit HO. Organization and in vitro activity of microfilament bundles associated with the basement membrane of Drosophila follicles. Acta Histochem Suppl. 1991; 41:201–10. [PubMed: 1811256]
13. Bateman J, Reddy RS, Saito H, Van Vactor D. The receptor tyrosine phosphatase Dlar and integrins organize actin filaments in the Drosophila follicular epithelium. Curr Biol. 2001; 11:1317–27. [PubMed: 11553324]
14. Prasad M, Jang AC, Starz-Gaiano M, Melani M, Montell DJ. A protocol for culturing Drosophila melanogaster stage 9 egg chambers for live imaging. Nat Protoc. 2007; 2:2467–73. [PubMed: 17947988]

15. Prasad M, Montell DJ. Cellular and molecular mechanisms of border cell migration analyzed using time-lapse live-cell imaging. Dev Cell. 2007; 12:997–1005. [PubMed: 17543870]
16. Oda H, Tsukita S. Real-time imaging of cell-cell adherens junctions reveals that Drosophila mesoderm invagination begins with two phases of apical constriction of cells. J Cell Sci. 2001; 114:493–501. [PubMed: 11171319]
17. Martin AC. Pulsation and stabilization: Contractile forces that underlie morphogenesis. Dev Biol. 2009
18. Martin AC, Gelbart M, Fernandez-Gonzalez R, Kaschube M, Wieschaus EF. Integration of contractile forces during tissue invagination. J Cell Biol. 2010; 188:735–49. [PubMed: 20194639]
19. David DJ, Tishkina A, Harris TJ. The PAR complex regulates pulsed actomyosin contractions during amnioserosa apical constriction in Drosophila. Development. 2010; 137:1645–55. [PubMed: 20392741]
20. Blanchard GB, Murugesu S, Adams RJ, Martinez-Arias A, Gorfinkiel N. Cytoskeletal dynamics and supracellular organisation of cell shape fluctuations during dorsal closure. Development. 2010; 137:2743–52. [PubMed: 20663818]
21. Edwards KA, Demsky M, Montague RA, Weymouth N, Kiehart DP. GFP-moesin illuminates actin cytoskeleton dynamics in living tissue and demonstrates cell shape changes during morphogenesis in Drosophila. Dev Biol. 1997; 191:103–17. [PubMed: 9356175]
22. Uehata M, et al. Calcium sensitization of smooth muscle mediated by a Rho-associated protein kinase in hypertension. Nature. 1997; 389:990–4. [PubMed: 9353125]
23. Hilgers RH, Webb RC. Molecular aspects of arterial smooth muscle contraction: focus on Rho. Exp Biol Med (Maywood). 2005; 230:829–35. [PubMed: 16339747]
24. Pellegrin S, Mellor H. Actin stress fibres. J Cell Sci. 2007; 120:3491–9. [PubMed: 17928305]
25. Narumiya S, Ishizaki T, Uehata M. Use and properties of ROCK-specific inhibitor Y-27632. Methods Enzymol. 2000; 325:273–84. [PubMed: 11036610]
26. Frydman HM, Spradling AC. The receptor-like tyrosine phosphatase lar is required for epithelial planar polarity and for axis determination within drosophila ovarian follicles. Development. 2001; 128:3209–20. [PubMed: 11688569]
27. Conder R, Yu H, Zahedi B, Harden N. The serine/threonine kinase dPak is required for polarized assembly of F-actin bundles and apical-basal polarity in the Drosophila follicular epithelium. Dev Biol. 2007; 305:470–82. [PubMed: 17383630]
28. Viktorinova I, Konig T, Schlichting K, Dahmann C. The cadherin Fat2 is required for planar cell polarity in the Drosophila ovary. Development. 2009; 136:4123–32. [PubMed: 19906848]
29. Mirouse V, Christoforou CP, Fritsch C, St Johnston D, Ray RP. Dystroglycan and perlecan provide a basal cue required for epithelial polarity during energetic stress. Dev Cell. 2009; 16:83–92. [PubMed: 19154720]
30. Brown NH, et al. Talin is essential for integrin function in Drosophila. Dev Cell. 2002; 3:569–79. [PubMed: 12408808]
31. Conway WC, et al. Paxillin modulates squamous cancer cell adhesion and is important in pressure-augmented adhesion. J Cell Biochem. 2006; 98:1507–16. [PubMed: 16552730]
32. Schaller MD. Paxillin: a focal adhesion-associated adaptor protein. Oncogene. 2001; 20:6459–72. [PubMed: 11607845]
33. Millan J, et al. Adherens junctions connect stress fibres between adjacent endothelial cells. BMC Biol. 2010; 8:11. [PubMed: 20122254]
34. Kee YS, Robinson DN. Motor proteins: myosin mechanosensors. Curr Biol. 2008; 18:R860–2. [PubMed: 18812080]
35. Kovacs M, Thirumurugan K, Knight PJ, Sellers JR. Load-dependent mechanism of nonmuscle myosin 2. Proc Natl Acad Sci U S A. 2007; 104:9994–9. [PubMed: 17548820]
36. Fernandez-Gonzalez R, Simoes Sde M, Roper JC, Eaton S, Zallen JA. Myosin II dynamics are regulated by tension in intercalating cells. Dev Cell. 2009; 17:736–43. [PubMed: 19879198]
37. Ren Y, et al. Mechanosensing through cooperative interactions between myosin II and the actin crosslinker cortexillin I. Curr Biol. 2009; 19:1421–8. [PubMed: 19646871]

38. Ewald AJ, Brenot A, Duong M, Chan BS, Werb Z. Collective epithelial migration and cell rearrangements drive mammary branching morphogenesis. Dev Cell. 2008; 14:570–81. [PubMed: 18410732]

39. Dietzl G, et al. A genome-wide transgenic RNAi library for conditional gene inactivation in Drosophila. Nature. 2007; 448:151–6. [PubMed: 17625558]

40. Delon I, Brown NH. The integrin adhesion complex changes its composition and function during morphogenesis of an epithelium. J Cell Sci. 2009; 122:4363–74. [PubMed: 19903692]

41. Vincent L, Soille P. Watersheds in Digital Spaces - an Efficient Algorithm Based on Immersion Simulations. Ieee Transactions on Pattern Analysis and Machine Intelligence. 1991; 13:583–598.

42. McDonald JA. M. D. Analysis of cell migration using Drosophila as a model system. Methods Mol Biol. 2005:175–202. [PubMed: 15576913]

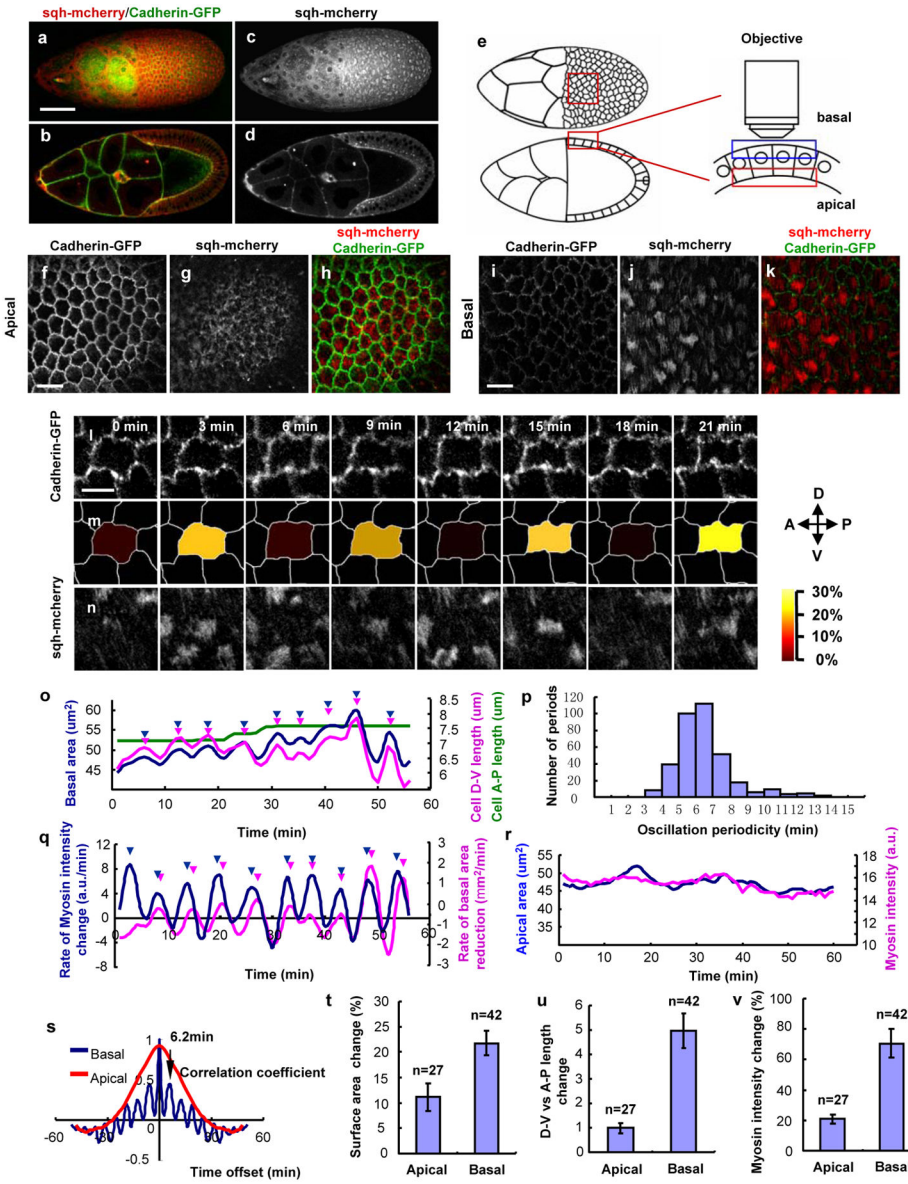

Figure 1. Stage 9 follicle cells undergo rapid, periodic contractions and myosin accumulation

a. Surface view of a live, late stage 9 egg chamber expressing Sqh-mcherry (red) and Cadherin-GFP (green). **b.** A sagittal plane through the center of the egg chamber. **c, d.** The Sqh-mcherry label alone. Scale bar is 50μm. **e.** Schematic drawings of egg chambers in **(a)** and **(b),** and the imaging of the apical and basal regions of the follicle cells. The red box at the left panel indicates a typical field of cells. The blue and red boxes indicate the basal and apical focal planes, respectively. **f–k.** Images of late stage 9 egg chamber expressing Sqh-mcherry (red) and Cadherin-GFP (green) at apical and basal focal planes, scale bar is 20μm. **l–n.** Time-lapse series of one representative oscillating cell labeled with Cadherin-GFP **(i)** and Sqh-mcherry **(n)**. The digitized cell contour is color coded based on the percentage of surface area reduction relative to the maximum area captured during imaging as indicated in the heat map **(m)**. Scale bar is 10μm. The A-P and D-V orientation is shown on the right.

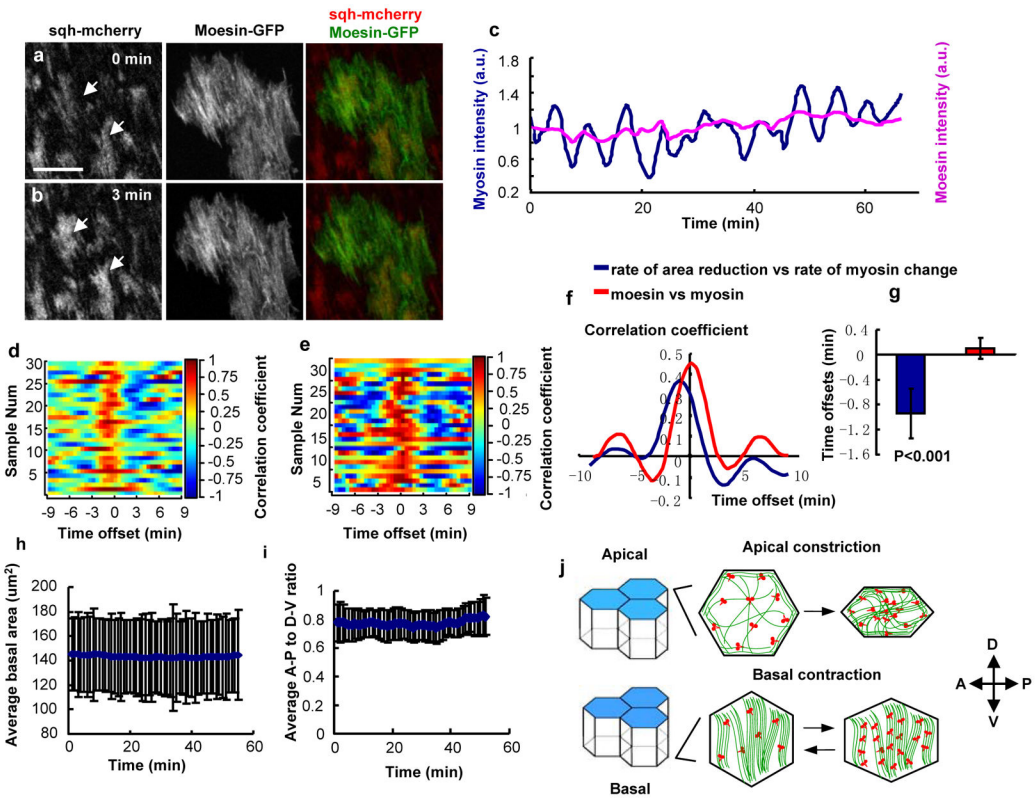

Figure 2. Quantification of basal periodic contraction and comparison with apical activity

a. Dynamic change of basal area, D-V and A-P cell length from one representative cell. Peaks are indicated by arrowheads of the corresponding color. **b.** The distribution of periods observed over 375 oscillations with mean at 6.3 min and standard deviation (s.d.) of 1.2 min. **c.** Change of apical area and apical myosin intensity from one representative cell over time. **d.** Calculated surface area change for the indicated numbers (**n**) of cells over 30 min of imaging. **e.** Calculated ratio of D-V to A-P length change over time. n is the number of individual cells analyzed. **f.** Changes of apical and basal myosin intensity compared with the average intensity for each, over the time course. n is the number of individual cells analyzed. **g.** The rate of change of myosin intensity (blue) and rate of reduction of basal area (purple) from the same sample. Peaks are marked with arrowheads. **h.** Autocorrelation of time sequences of apical (red) and basal (blue) myosin intensity. All error bars indicate ± standard deviation.

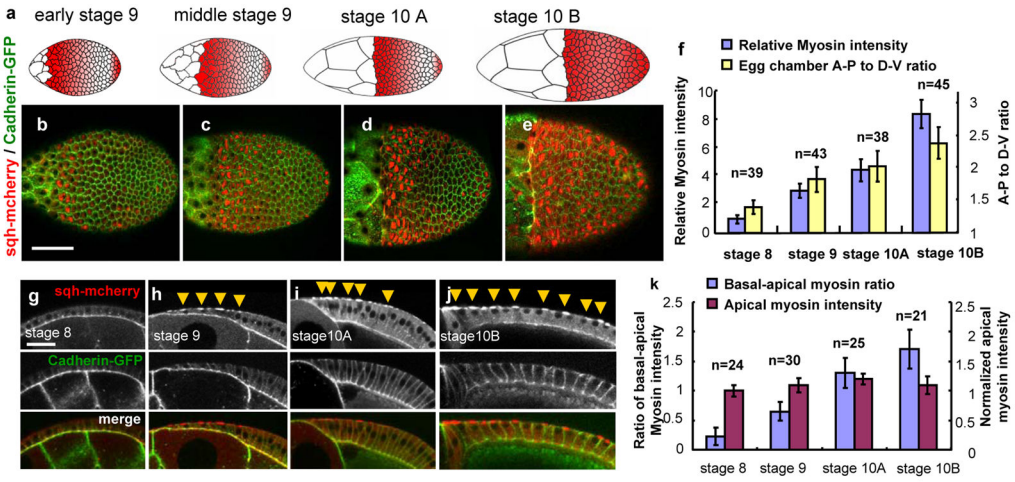

Figure 3. Accumulation of basal myosin on stable actin filaments precedes the basal membrane contraction

a, b. Confocal micrographs of a clone of Moesin-GFP in Sqh-mcherry expressing cells. Images in a and b were taken 3 minutes apart. Myosin intensity changes in two cells (left panel, arrows) whereas Moesin-labeled F-actin does not change detectably. Scale bar is 10μm**. c.** Quantification of the dynamic change of Moesin-GFP and Sqh-mcherry intensity in one oscillating cell. Intensity of each channel was normalized to its mean. **d.** Correlation between the rate of basal area reduction and myosin intensity change **e.** and Correlation between the rate of basal area reduction and moesin intensity. Each row shows the correlation from a different cell as a function of various time offsets. **f.** Average of all correlation coefficients with different time offsets. The red line shows the average time-dependent correlation between area reduction rate and myosin intensity rate from 43 individual cells. The blue line shows the average time-dependent correlation between moesin and myosin intensity from 37 individual cells. The correlation between the rate of basal area reduction and myosin accumulation reaches maximum at −1 min, suggesting that myosin accumulation precedes area reduction. In contrast, the correlation between myosin intensity and F-actin intensity peaks at 0, indicating that they are virtually simultaneous. **g.** The position of maximum correlation between contraction rate and intensity change rate (blue) is significantly different from zero with $p<0.001$, while the moesin and myosin correlation (red) is not. Error bars indicate ±s.d. **h.** The basal areas of cells (n=45) were calculated and averaged. Even though the basal areas of individual cells fluctuated periodically, the average basal area did not change because the fluctuations were temporary and unsynchronized. **i.** The ratio of A-P to D-V cell lengths during the time of imaging. n=45. The periodic changes observed in individual cells were neither synchronous nor lasting, therefore no change was detected on average. **j.** Diagram of different organizations and dynamics of the apical actomyosin for cells undergoing apical constriction vs. the basal actomyosin for cells undergoing basal oscillations.

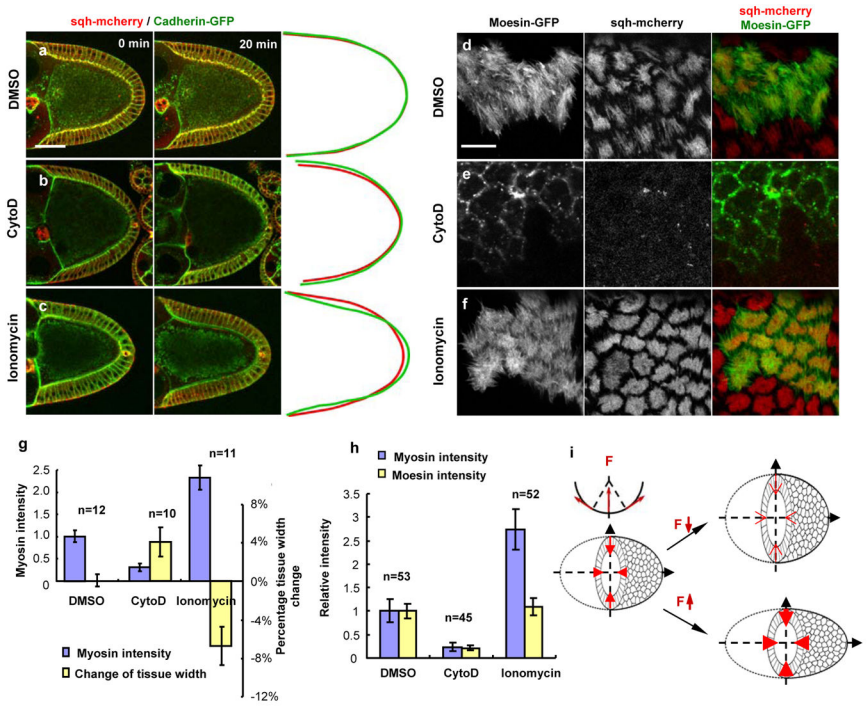

Figure 4. Global change of basal myosin during egg chamber development

a. Schematic drawings of egg chambers at indicated developmental stages. Red shading illustrates the overall distribution of cells with periodic myosin accumulation. Anterior is to the left. **b–e.** Live egg chambers expressing Sqh-mcherry and Cadherin-GFP at early stage 9 **(b)**, middle stage 9 **(c)**, stage 10A **(d)**, and stage 10B **(e)**. Scale bar is 50μm. **f.** Basal myosin intensity relative to stage 8 and ratio of A-P to D-V egg chamber length at different stages. A-P or D-V length was defined as the maximum distance between two points of the tissue in corresponding direction. **g–j.** Side views of follicle cells from egg chambers of the indicated stages show the increase of basal myosin and comparatively constant apical myosin through development. Arrows indicate sites of basal myosin accumulation. Scale bar is 15 μm. **k.** Apical myosin intensity normalized to stage 8 and the ratio of basal myosin intensity (in cells that exhibit basal myosin accumulation) to apical myosin in the indicated number (n) of cells from stages 8 to 10.

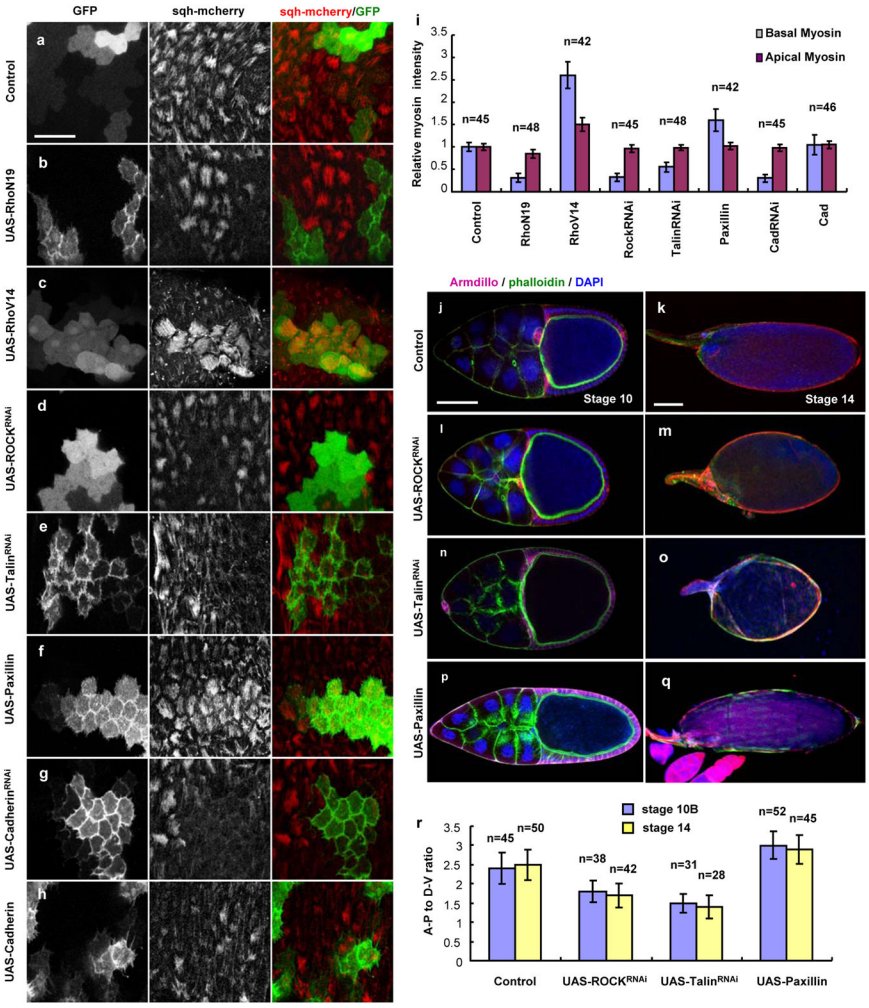

Figure 5. Basal actomyosin contractions control tissue shape

a–c. Confocal micrographs of egg chambers treated with vehicle (DMSO), cytoclasin D (CytoD), or ionomycin at 0 min (the beginning of imaging) and 20 min. Tissue contours at the two time points are outlined in red (0 min) and green (20 min) lines. Scale bar is 50 μm. Control experiments and combination effects are shown in Supplementary Information, Fig. S3h-q. **d–f.** Live images of basal F-actin (labeled with Moesin-GFP) and myosin (Sqh-mcherry) after 30 min treatment with DMSO, CytoD or ionomycin. Scale bar is 10μm. Over 80% reduction of basal Moesin-GFP signal after CytoD treatment (**e**) suggested the majority GFP intensity represents F-actin. Ionomycin showed little or no effect on basal F-actin (**f**). Treatment with ROCK and calcium inhibitors reduced myosin intensity to near background but had little effect on actin (Supplementary Information, Fig. S3a–c), suggesting that the formation of basal actin and myosin contractile fibers is regulated independently. **g.** Average basal myosin intensity and the percentage change of egg chamber width during the 20 min imaging time following treatment with the indicated drugs. n is the number of the samples analyzed. **h.** Quantification of basal Moesin-GFP and myosin intensity after treatment with the indicated drugs. n is the number of cells analyzed. All error bars indicate ±s.d. **i.** An illustration of the proposed mechanism by which follicle cell relaxation or contraction leads

to tissue rounding or elongation. Due to curvature of the egg chamber, contractile force (F) generated at the basal side is exerted in part toward the center. The red arrowheads indicate different magnitudes of contractile forces.

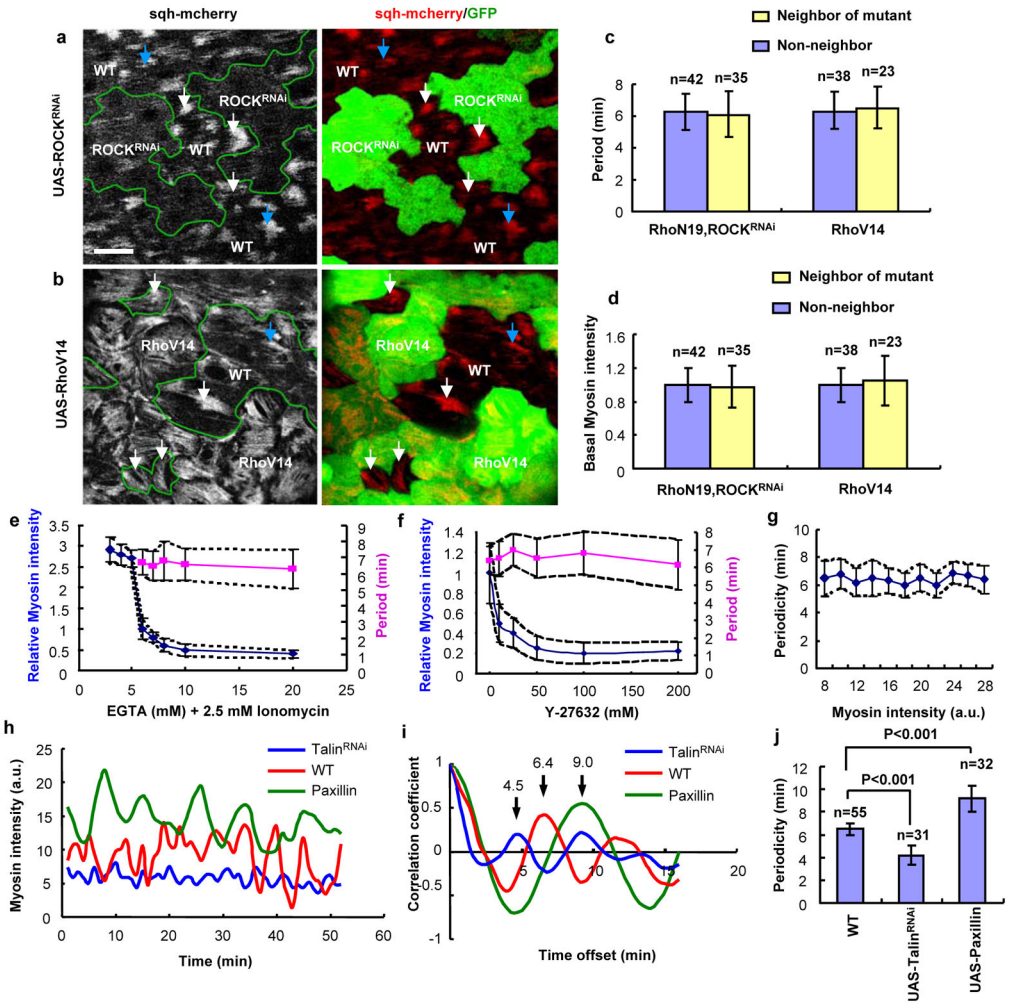

Figure 6. Rho, ROCK and cell adhesion regulate basal myosin accumulation and organ shape

a–h. Basal view of follicle cell clones expressing the indicated transgenes, marked by coexpression of either nlsGFP or mCD8GFP. Scale bar is 20μm. **i.** Quantification of relative basal and apical myosin intensity in the indicated number (n) of GFP positive cells compared with wild type cells in the same sample. Corresponding apical myosin and apical and basal actin images are shown in Supplementary Information, Fig. S4, S5. Verification of RNAi knock-down and over-expression are shown in Supplementary Information, Fig. S6**. j–q.** Morphology of stage 10B (**j, l, n, p**) and stage 14 (**k, m, o, q**) egg chambers expressing the indicated transgene in all follicle cells. Egg chambers expressing *hs*Gal4 served as controls. Scale bar is 50 μm. **r.** Quantification of the A-P vs D-V length ratio at stage10B and 14 egg chambers with indicated genetic backgrounds. n is the number of samples analyzed. In contrast, no significant difference was observed at late stage 8 (Supplementary Information, Fig. S7). All error bars are ±s.d.

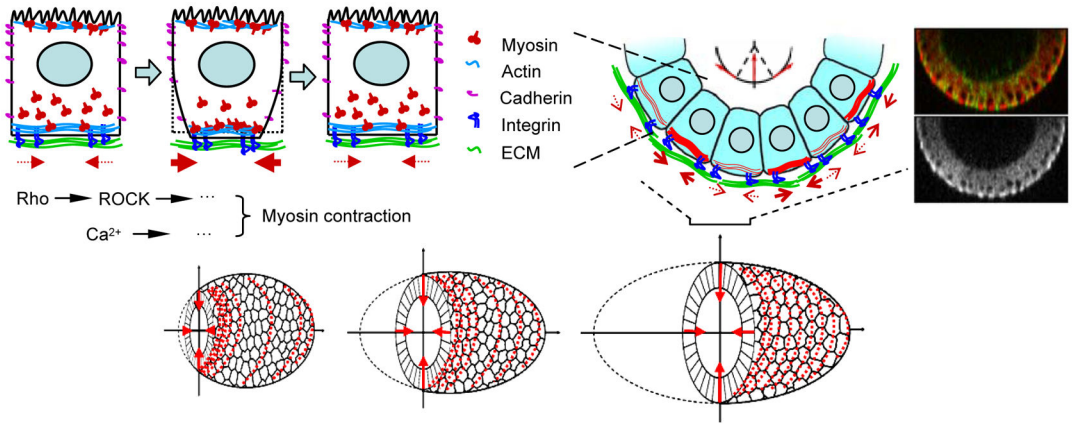

Figure 7. Cell autonomy of myosin oscillation and pathways affecting its magnitude and period

a, b. Confocal micrographs of follicle cell clones in living egg chambers expressing Sqh-mcherry. **a.** Wild type (WT, GFP-negative) cells adjacent to cells expressing ROCK RNAi (GFP-positive) are indicated by white arrows. WILD TYPE cells without any contact with ROCK RNAi-expressing cells are indicated by blue arrows. Scale bar is 10μm. **b.** Wild type (WT, GFP-negative) cells adjacent to cells expressing RhoV14 (GFP-positive) are indicated by white arrows. A wild type cell without any contact with RhoV14 -expressing cells is identified by a blue arrow. **c, d.** Quantification of myosin intensity and oscillation period in wild type cells that neighbor mutant cells showed no significant difference from wild type cells that did not neighbor mutant cells. n is the number of individual cell analyzed. **e.** Basal myosin intensity and oscillation period after addition of different concentrations of EGTA together with 2.5 μM ionomycin. 48 individual cells were analyzed covering ~150 periods. **f.** Basal myosin intensity and oscillation period after treatment with various concentrations of the ROCK inhibitor Y-27632. 37 cells were analyzed covering ~110 periods. **g.** Plot of oscillation period vs basal myosin intensity in wild type egg chambers. Samples were collected from 65 individual cells covering more than 200 periods. **h.** Dynamics of basal myosin intensity in a representative individual cell expressing UAS-talin RNAi, UAS-paxillin, or no UAS transgene (WT). **i.** The autocorrelation with different time offsets from data in (**h**). The first peak for each line provides the period for the corresponding genotype. **j.** Quantification of the effect on period. n is the number of cells from three independent clones analyzed. All error bars indicate ±s.d.

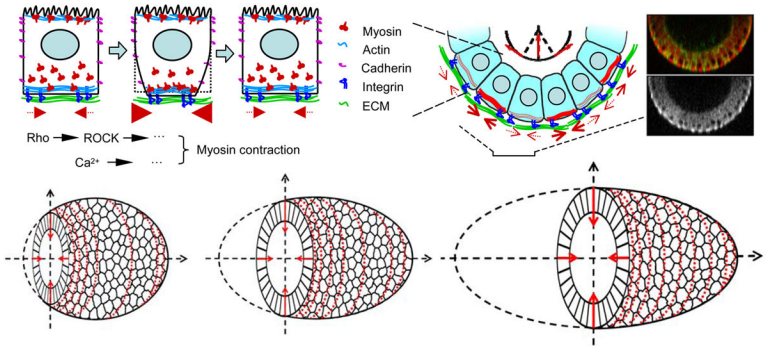

Figure 8.

Model of tissue elongation controlled by basal actomyosin contraction Schematic representation of the distribution of molecules controlling oscillating basal contraction in an individual follicle cell and the organization of contractile forces into a super cellular band within the epithelium. Forces are indicated by red arrows. Local contraction force generated by basal myosin (red) transmitted through adhesions (blue) to the basal lamina (cyan) constrains tissue growth to the poles. Micrographs show a corresponding section through the middle of a stage 10 egg chamber labeled with cadherin-GFP;sqh-mcherry. The sqh-mcherry channel only is shown in black and white.